Determination of two-dimensional phonon dispersion relation of graphite by Raman spectroscopy

A. Grüneis,[1] R. Saito,[1] T. Kimura,[1] L. G. Cançado,[2] M. A. Pimenta,[2] A. Jorio,[2,3] A. G. Souza Filho,[3,4] G. Dresselhaus,[5] and M. S. Dresselhaus[3,6]

[1]*Department of Electronic-Engineering, University of Electro-Communications, Chofu, Tokyo 182-8585, Japan*

[2]*Departamento de Física, Universidade Federal de Minas Gerais, Belo Horizonte, Minas Gerais 30123-970, Brazil*

[3]*Department of Physics, Massachusetts Institute of Technology, Cambridge, Massachusetts 02139-4307*

[4]*Departamento de Física, Universidade Federal do Ceará, Fortaleza, Ceará 60455-760, Brazil*

[5]*Francis Bitter Magnet Laboratory, Massachusetts Institute of Technology, Cambridge, Massachusetts 02139-4307*

[6]*Department of Electrical Engineering and Computer Science, Massachusetts Institute of Technology, Cambridge, Massachusetts 02139-4307*

Phonon dispersion relations of a two-dimensional (2D) graphite are obtained by fitting dispersive Raman modes that originate from nonzone center phonons near the Γ or K point in the Brillouin zone (BZ). A new set of 12 force constants of 2D graphite up to the fourth neighbor are determined by a self-consistent fitting procedure, combined with double-resonance Raman theory. Analytical expressions for eigenvalues and eigenvectors at high symmetry points of the BZ are presented.

I. INTRODUCTION

Phonon energy dispersion relations are a fundamental physical property of a solid especially for determining the mechanical, thermal, and other condensed-matter phenomena. The phonon energy dispersion of three-dimensional (3D) graphite (or two-dimensional (2D) turbostratic graphite) have been determined experimentally by inelastic neutron scattering[1,2] and electron-energy-loss spectroscopy (EELS).[3,4] Theoretically a tight-binding force-constant model (or a molecular-dynamics method) has been adopted for describing phonon energy dispersion in which a set of 8 or 12 force constants are able to reproduce the phonon energy dispersion over the Brillouin zone (BZ).[5–7] Using the 12 force-constant parameters, we have calculated the phonon dispersion relations of single-wall carbon nanotubes (SWNTs).[5,8] Such a result has wide applicability for use in analyzing the Raman spectra of SWNTs.[9] However, inelastic neutron scattering or EELS measurements are, in general, not suitable for observing phonon dispersion relations of SWNTs directly, since a bundle of SWNTs is not a single crystal, but consists of many different chiralities and diameters of SWNTs. Further, inelastic neutron scattering is known to be unsuitable for observing phonon modes at the zone boundary.

Recently double-resonance Raman spectra have probed the phonon dispersion relations of 2D graphite.[10] So far, Raman spectroscopy does not provide the phonon dispersion relations because the wave vector of the incoming photon is too small to create phonons at a large distance from the Γ point in the first-order Raman scattering process. Thus only zone-center Raman modes are observed, in general, in crystalline solids from the first-order spectra. However, in second-order Raman scattering processes, there are low-intensity features in the Raman spectra, which do not originate from the Γ point. These peaks in the second-order Raman spectra can be classified into two-phonon peaks and disorder-induced one-phonon peaks. It is easy to distinguish most second-order Raman peaks from first-order features, since the Raman mode frequencies of the second-order Raman processes are generally dispersive, that is, the frequencies depend on the laser excitation energy E_{laser}. An example of a disorder-induced phonon mode is the D band around 1350 cm^{-1} for laser excitation energy $E_{laser}=2.41$ eV.[9,11–16] This mode shifts with laser excitation energy by about 53 cm^{-1}/eV. The overtone mode of the D band is known as the G' band[12] (or the D^* band using another notation[16]) at about 2700 cm^{-1} with a dispersion of about 106 cm^{-1}/eV. The G'-band spectrum is visible even in highly ordered graphite, since the corresponding process involves the creation of two phonons with equal but oppositely directed momenta.

Thomsen and Reich explained the dispersion of the D-band phonon frequency with E_{laser} by a double-resonance process.[15] This idea was then applied to all six branches of the phonon dispersion relations of graphite, for which many disorder-induced peaks can be assigned as nonzone center phonon modes when combined with the theory.[10] The assignment is almost perfect near the Γ point. However, the assignment is not so good near the K point (hexagonal corners of the 2D BZ), which is ascribed to the lack of experimental data from inelastic neutron measurements for regions of the Brillouin zone near the K point. In this paper, using double-resonance Raman data, we fit the phonon dispersion relations over the whole 2D BZ. Further, in order to discuss non-zone-center Raman modes, the vibrational motion at the high symmetry points is investigated. In particular, we present analytical results for the eigenvalues and eigenvectors, which can then be used in the fitting procedure and mode analysis.

In the following section, we present a brief overview of double-resonance phenomena associated with second-order Raman scattering. In Sec. III, we explain the fitting procedure and analytical expression for the dynamical matrix eigenvalues that we used to obtain the phonon dispersion relations. In Sec. IV we present the calculated results of the phonon dispersion relations, a new set of force constants, and
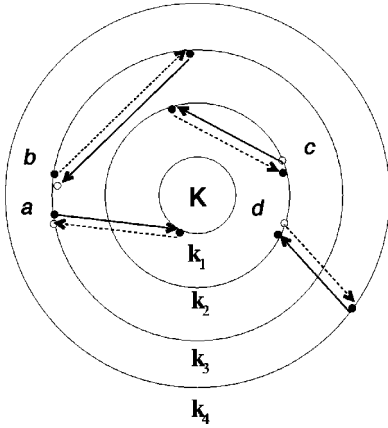
FIG. 1. Four different, intravalley, double-resonance scattering processes occur around the K point in the 2D Brillouin zone of graphite. At each point of a, b, c, and d, an electron-hole pair is created. The electron is then scattered, and subsequently backscattered to the original position. Solid and dotted lines are, respectively, inelastic and elastic scattering processes. In a and c, inelastic scattering occurs first, while in b and d, elastic scattering occurs first. Solid and open circles denote resonant and nonresonant states, respectively. Processes a and b, and c and d correspond, respectively, to incident and scattered resonance conditions. Four energy surfaces correspond to the energies from the smallest energy (or circle), $E_{laser}/2 - E_{phonon}$, $E_{laser}/2 - E_{phonon}/2$, $E_{laser}/2$, and $E_{laser}/2 + E_{phonon}/2$, for which the k vectors are denoted by k_1 to k_4, respectively. The separation between two circles is artificially enlarged for clear understanding.

analytic expressions for the eigenvalues and eigenvectors of the dynamical matrix, and in Sec. V a summary is given.

II. DOUBLE-RESONANCE RAMAN SPECTRA

In the double-resonance Raman processes, the origin of the D band and of the many weak dispersive phonon modes in the Raman spectra of graphite is explained by (1) a second-order scattering process, and (2) a resonant enhancement of the Raman intensity in two consecutive scattering processes. In the second-order scattering process, an electron with initial momentum k is (a) at first excited to the energy $E^i(k)$ by the incident photon, (b) scattered to a state $k + q,[E(k+q)]$, and (c) then backscattered to the state $k,[E^f(k)]$, and finally (d) recombined with a hole to yield the scattered photon. If $E(k+q)$ and either the $E^i(k)$ or $E^f(k)$ states correspond to real electronic states, the Raman intensity is enhanced by two resonant factors in the denominators occurring in the intensity formula, and this is known as the double-resonance Raman process.[17]

When we look at double-resonance Raman processes in the 2D BZ of graphite, we see that electrons around the K point are relevant to Raman processes. As far as we restrict the exciting laser energies E_{laser} to be $E_{laser} < 3$ eV, the equienergy contours of π electrons can be treated as circles around the K point as a first approximation (see Fig. 1). Further we assume that the electron energy dispersion is symmetric $\pm E(k)$ around the Fermi energy $E = 0$, where $E(k)$ and $-E(k)$ are antibonding π^* and bonding π bands,

respectively. Here we adopt a simple tight-binding result for $E(k)$ (Ref. 5) with a nearest-neighbor tight-binding parameter $\gamma_0 = 2.89$ eV. For smaller laser energies, we can use the linearized energy dispersion relation for electrons, $E(k) = \sqrt{3}\gamma_0 ka/2$ in which a is the lattice constant $a = \sqrt{3}a_{C-C}$ with $a_{C-C} = 1.42$ Å. In this case the photon absorption occurs when $E_{laser} = 2E(k)$. Hereafter the k vectors which exist on the energy contour $E = E(k)$ are denoted by $k = k(E)$. When we consider double-resonance Raman processes involving an inelastic scattering event by emitting a phonon with energy E_{phonon} and an elastic scattering event due to an impurity occurring for each forward and backscattering event, we have four different resonant processes. A factor of 2 (out of the factor 4) comes from two possibilities: whether inelastic or elastic scattering occurs first, and another factor of 2 comes from whether the incident $E^i(k)$ or the scattered $E^f(k)$ states are resonant. These four processes generally lead to different lengths from one another for the wave vector q of the scattering phonon. Moreover, there are two possibilities for selecting the q vectors, since there are two inequivalent energy contours around the K and K' points in 2D BZ. A relatively small q vector is selected for scattering within the same energy contour (from K to K or from K' to K'), while a larger q vector is selected for scattering from K to K' (or from K' to K), which we call intravalley and inter valley scattering, respectively. In total, there are eight different double-resonance Stokes scattering processes for the second-order, one-phonon emission, double-resonance D-band Stokes processes.

In Fig. 1 we show an example of the four q vectors for intravalley scattering, where solid and dotted arrows denote inelastic and elastic scattering processes, respectively. Solid and open small circles denote, respectively, resonant and nonresonant conditions. In the case of the solid circles, the corresponding energy of the state is that for $E(k)$, while the state for open circles has an energy different from $E(k)$. The electron-hole pair is created and recombined for the same k points next to the labels corresponding to the processes a, b, c, or d. From this point the electron is scattered to an intermediate $k + q$ state, which is always resonant (one solid circle). In the case of processes a and b, the incident laser with E_{laser} is in resonance with $E^i(k)$ and solid circles of a and b correspond to the initial states. Thus the initial k vectors are on the second largest circle of the energy contour of $E = E_{laser}/2$. In the case of a, the scattering to the intermediate state is inelastic (solid arrow), and the corresponding energy lies on the smallest circle where $E = E_{laser}/2 - E_{phonon}$. The backscattering to k now becomes elastic and $E^f(k) = E_{laser}/2 - E_{phonon}$ is smaller than $E^i(k)$ which is denoted by an open circle. In the case of b, the scattering to the intermediate states is elastic and thus the intermediate states are on the same circle as the initial states. The backscattering to the initial states for b is inelastic and $E^f(k)$ is nonresonant and has an energy $E_{laser}/2 - E_{phonon}$.

For processes c and d, the final states with $E^f(k)$ are resonant with the scattered energy $E_{laser} - E_{phonon}$ and thus the final k vectors are selected on $k(E_{laser}/2 - E_{phonon}/2)$, which are the second smallest circles in Fig. 1. The corre-
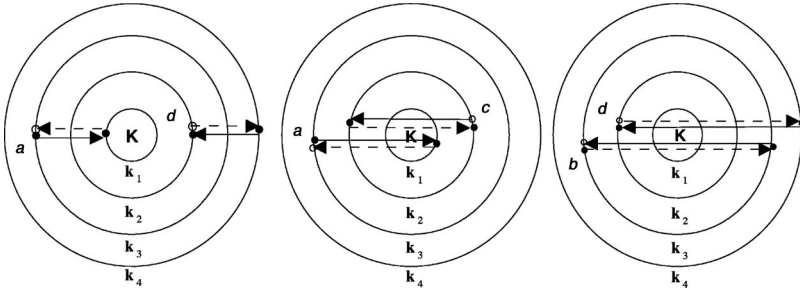
FIG. 2. Here the three extreme cases, which lead to a high density of q vectors for intravalley scattering are shown. The left figure corresponds to $\mathbf{q} \sim 0$ for a and d in Fig. 1 and the center and the right figures correspond, respectively, to the $q \sim 2k$ and $q = 2k$ cases for a and c and for b and d.

sponding initial $\mathbf{k}$ vectors for c and d lie on the circles $k(E_{\text{laser}}/2 - E_{\text{phonon}}/2)$. In the case of c, since the backscattering is elastic, the intermediate states should have the same energy as $E^f(\mathbf{k})$, while in the case of d, the backscattering is inelastic and thus the intermediate state has a higher energy than the final state by the phonon energy, namely, $E_{\text{laser}}/2 + E_{\text{phonon}}/2$.

Thus we can classify the four processes by either an incident or scattered resonance Raman event, and by the fact that either the elastic or the inelastic event occurs first: a incident resonance, inelastic first, b incident resonance, elastic first, c scattered resonance, inelastic first, and d scattered resonance, elastic first. As a result, four electron energy contours separated by $E_{\text{phonon}}/2$ are relevant for the double-resonance processes, as shown in Fig. 1. Thus four energy surfaces correspond to the energies from the smallest energy (or circle) in Fig. 1, $E_{\text{laser}}/2 - E_{\text{phonon}}$, $E_{\text{laser}}/2 - E_{\text{phonon}}/2$, $E_{\text{laser}}/2$, and $E_{\text{laser}}/2 + E_{\text{phonon}}/2$, for which the $\mathbf{k}$ vectors are denoted by k_1 to k_4, respectively. It is noted here that E_{phonon} ($\leqslant 0.15$ eV) is generally much smaller than E_{laser} ($2 \sim 3$ eV) so that the distance between two of the circles $\delta k = k(E_{\text{phonon}}/2)$ is smaller than the diameter of the circles and much smaller than the hexagonal edge of the 2D BZ. Figure 1 is drawn schematically to convey a clear understanding of the physical processes.

The phonon $\mathbf{q}$ vectors for the intravalley scattering are related to phonon wave vectors around the Γ points. In the case of intervalley scattering, the intermediate $\mathbf{k}+\mathbf{q}$ states exist at inequivalent K' points with the same energy as in Fig. 1. The corresponding $\mathbf{q}$ vector has a value from K to K' (or from Γ to K). The $\mathbf{q}$ vectors for the intervalley scattering are related to those around the K point.[10]

For any $\mathbf{k}$ vector, possible $\mathbf{q}$ vectors exist on the circle of the $\mathbf{k}+\mathbf{q}$ states for each case, and the length of the $\mathbf{q}$ vectors can be changed from the closest to the most distant points on the circles. Since we can assume that the $\mathbf{q}$ vectors are homogeneously distributed on the 2D BZ, and especially on the circles, the density of the distance of $\mathbf{q}$ vectors from the K point, has a singularity for $|\mathbf{q}|$ at the minimum and the maximum points, which are shown in Fig. 2. The maximum $|\mathbf{q}|$ vector corresponds to $2|\mathbf{k}|$ if we neglect the small difference between the diameters of the circles, as mentioned above. In the case of the minimum $|\mathbf{q}|$ values, we can assume $|\mathbf{q}| = 0$, which is exact for b and c. Since the phonon dispersion, except for the acoustic phonon mode, is flat around $|\mathbf{q}| = 0$, the minimum $|\mathbf{q}| \sim 0$ also gives a phonon frequency similar to that of $|\mathbf{q}| = 0$. It is clear that the lengths of the $\mathbf{q}$ vectors are equal for the two processes of each figure. This gives two

split peaks in the dispersive phonon modes for $|\mathbf{q}| \neq 0$ and one peak for $|\mathbf{q}| = 0$ when the distance is measured from the Γ and K points for intravalley and intervalley scattering, respectively. Recent Stokes and anti-Stokes experimental spectra observed for the D band in disordered graphite can be decomposed into two Lorentzians.[18] However, in the following analysis of the fitting procedure of the phonon dispersion relations, we treat each peak as an average value. In fact, since the error bar for the fitting procedure is larger than the splitting, we can neglect the D-band splitting in the first approximation.

III. FITTING PROCEDURE AND ANALYTICAL SOLUTION METHOD

For a given energy of E_{laser}, we can select $|\mathbf{k}|$ values by using the electronic energy dispersion relations of 2D graphite, and then we can specify the phonon $|\mathbf{q}| = 2|\mathbf{k}|$ or 0 vectors measured from the Γ and K points. The observed weakly dispersive phonon modes should be on the phonon dispersion relations corresponding to $|\mathbf{q}|$ values near the Γ point. Here we fit experimental data to the calculated phonon dispersion relations, which are calculated by a molecular dynamics method in which the dynamical matrix is solved using 12 force constants, up to fourth neighbor carbon atoms.[5,8] We then perform a nonlinear least squares fit for the force-constant vector $\mathbf{f}$ which minimizes the least-squares value of $S(\mathbf{f})$,

$$S(\mathbf{f}) = \sum_{i,n}^{I,N(i)} A_{i,n}\{\omega_{i,n}^{\text{obs}} - \omega^{\text{calc}}(\mathbf{q}_{i,n}, \mathbf{f})\}^2, \quad (1)$$

where $\omega_{i,n}^{\text{obs}}$ and $\omega_{i,n}^{\text{calc}}(\mathbf{q}_{i,n}, \mathbf{f})$ are the observed and calculated phonon frequencies, respectively. Here the index i in the sum runs over the phonon branches, and the index n runs over the points in the i-th phonon branch whose number is $N(i)$. The least-squares value from each point is multiplied by the weight $A_{i,n}$. If we give a larger weight to one point, we can increase the importance of that point. The weight is used to include an experimental error or to increase the quality of the fit near points that are considered to be important, e.g., the zone-center modes or the modes pertinent to the D band. Although there exists some ambiguity in assigning the weight $A_{i,n}$, it is necessary to make such an assignment to get good convergence for the inhomogeneously distributed experimental data.
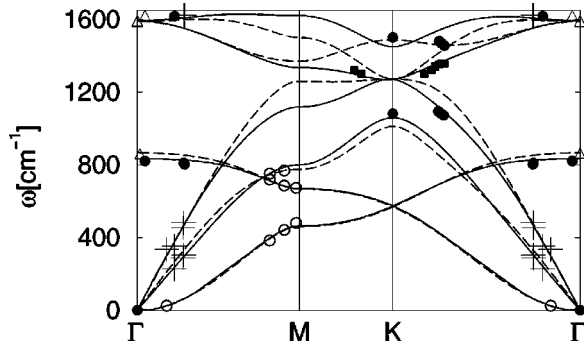
FIG. 3. Fitted phonon dispersion relations (solid lines) for 2D graphite. The dashed lines are the previous phonon dispersion relation fitted to inelastic neutron scattering measurements (Refs. 1, 5 and 25). Solid dots, solid squares, crosses, and triangles are Raman data of highly ordered pyrolytic graphite (HOPG), Refs. 19 and 20, single-wall carbon nanotube (SWNT), Ref. 16, HOPG and SWNT (Ref. 22) and graphite whisker (GW), Ref. 21, respectively. Open circles are inelastic neutron scattering data for graphite, Ref. 5.

The phonon **q** vectors are selected by calculating the density of $|\mathbf{q}|$ vectors, which satisfy the energy momentum conservation law in the double resonance condition

$$E(\mathbf{k}+\mathbf{q}) = E(\mathbf{k}) - \hbar\,\omega(\mathbf{q},\mathbf{f}) \qquad (2)$$

and so on, for each of the four processes. Thus **q** and $\omega(\mathbf{q})$ are self-consistently solved in the sense that the $\omega(\mathbf{q})$ relation used for obtaining **q** in Eq. (2) becomes the same as that for fitting $\omega(\mathbf{q})$ to Eq. (1). The least-squares fit is obtained by linearizing $\omega_{i,n}^{\mathrm{calc}}(\mathbf{q},\mathbf{f})$ with respect to **f**, and the fit is accomplished when the input $\omega(\mathbf{q})$ and the fitted $\omega_{i,n}^{\mathrm{calc}}(\mathbf{q},\mathbf{f})$ are identical.

The force-constant vectors, eigenvalues, and eigenvectors at the high symmetry points are given by the converged results. We also did an analytical calculation using MATHEMATICA for obtaining the phonon frequency at the high symmetry points as a function of the force-constant vector. Such results are useful for obtaining the force-constant values from the phonon frequencies. The information on the eigenfunctions (normal modes) is useful for understanding the corresponding non-zone-center phonon modes.

IV. RESULTS

A. Numerical fitting of the phonon dispersion relations

In Fig. 3, the fitted phonon dispersion relations are shown by solid lines. The dashed lines are the phonon dispersion relations that are fitted to inelastic neutron scattering data. Solid dots, solid squares, crosses, and triangles are Raman data of highly ordered pyrolytic graphite (HOPG),[19,20] single-wall carbon nanotubes (SWNTs),[16] HOPG and SWNTs,[21] and graphite whisker (GW),[22] respectively. In order to improve the convergence of the iterative fitting, we have also used inelastic neutron scattering data (open circles in Fig. 3) in the low-frequency region near the M point that

TABLE I. Calculated force-constant parameters for 2D graphite in units of 10^4 dyn/cm. Here the subscripts r, ti, and to refer to radial, transverse in-plane and transverse out-of-plane, respectively. The previous force constants are listed in parentheses (Ref. 5).

Radial	Tangential	
$\phi_r^{(1)} = 40.37\,(36.50)$	$\phi_{ti}^{(1)} = 25.18\,(24.50)$	$\phi_{to}^{(1)} = 9.40\,(9.82)$
$\phi_r^{(2)} = 2.76\,(8.80)$	$\phi_{ti}^{(2)} = 2.22\,(-3.23)$	$\phi_{to}^{(2)} = -0.08\,(-0.40)$
$\phi_r^{(3)} = 0.05\,(3.00)$	$\phi_{ti}^{(3)} = -8.99\,(-5.25)$	$\phi_{to}^{(3)} = -0.06\,(0.15)$
$\phi_r^{(4)} = 1.31\,(-1.92)$	$\phi_{ti}^{(4)} = 0.22\,(2.29)$	$\phi_{to}^{(4)} = -0.63\,(-0.58)$

was used in the previous fitting.[5] The data points at the Γ point are taken from first-order Raman scattering, and those at the K point are taken from dispersionless weak features, which are assigned to $\mathbf{q}=0$ singular phonon modes. When we compare the phonon dispersion of the solid and dotted lines, only the higher-frequency region around the K point is different. In the lower-frequency region, the dispersive Raman data are in good agreement with the previous phonon dispersion relations. There are dispersive Raman data around 1050 cm^{-1}, which shift the longitudinal acoustic (LA) mode to a lower-frequency region. In the phonon dispersion relations obtained by inelastic neutron data, this LA mode is highly anisotropic around the K point. Since the double-resonance theory gives the phonon frequencies in terms of the distance from the K (or the Γ) point, we cannot determine the anisotropy of the phonon branches around the K point. However, no experimental inelastic neutron data are available near the K point, and the lowering of the LA curve from the Γ to the K point seems to be in good agreement with the experiment.

The second highest phonon dispersion branch around the K point gives the D-band frequency. The fitted phonon dispersion in Fig. 3 gives a smaller slope for the phonon dispersion relation than that given by the previous one. It should be mentioned that we excluded some experimental points for higher E_{laser} values on the K-M line. Along the K-M line the anisotropy of the phonon dispersion is large compared with the K-Γ line. Since our double-resonance model calculation only gives the distance of the **q** vector, which is the $|\mathbf{q}|$ value from the K point, the calculation might not be adequate for the fitting procedure for larger laser energies if there is a large anisotropy (~ 30 cm^{-1}) in the phonon dispersion relations for large $|\mathbf{q}|$. Such an anisotropy is known as the trigonal warping effect and the circles are modified to show an approximate triangular shape. In this case, since the edge section, which gives a singular $|\mathbf{q}|$ is given around the K-Γ line, the treatment that we give for the experimental points on the K-Γ line is justified. When D-band phonon data become available for smaller laser energies, it will be nice to have more reliable data around the K point (or the Γ point), which can then be used in a future study.

For use in future studies, we list in Table I an updated summary of the 12 fitted force constants in which $\Phi_r^{(n)}$, $\Phi_{ti}^{(n)}$, and $\Phi_{to}^{(n)}$ denote, respectively, the force constants of the radial, in-plane, and out-of-plane modes for the n-th nearest neighbor atoms ($n=1,\ldots,4$). Force constants up to fourth neighbor atoms are needed to reproduce the twisting vibra-

TABLE II. Eigenvectors R_A, R_B and frequencies in cm^{-1} are listed for in-plane ω_i and out-of-plane ω_o phonon modes at the $\Gamma=(0,0)$, $K=(2\pi/\sqrt{3}a, 2\pi/3a)$, and $M=(2\pi/\sqrt{3}a,0)$, points. (Note, $\alpha=e^{-\pi i/6}$, $\gamma=e^{2\pi i/3}$.)

Mode	Γ freq.	Γ $\{R_A, R_B\}$	K freq.	K $\{R_A, R_B\}$	M freq.	M $\{R_A, R_B\}$
ω_{i1}	1589	$\{(1,0,0),(-1,0,0)\}$	1487	$\{(\alpha, i\alpha, 0),(-i,-1,0)\}$	1500	$\{(\gamma,0,0),(-1,0,0)\}$
ω_{i2}	1589	$\{(0,1,0),(0,-1,0)\}$	1272	$\{(0,0,0),(-i,1,0)\}$	1369	$\{(0,\gamma,0),(0,1,0)\}$
ω_{i3}	0	$\{(1,0,0),(1,0,0)\}$	1272	$\{(i,1,0),(0,0,0)\}$	1259	$\{(\gamma,0,0),(1,0,0)\}$
ω_{i4}	0	$\{(0,1,0),(0,1,0)\}$	1011	$\{(\alpha, i\alpha, 0),(i,1,0)\}$	775	$\{(0,\gamma,0),(0,-1,0)\}$
ω_{o1}	865	$\{(0,0,1),(0,0,-1)\}$	568	$\{(0,0,1),(0,0,0)\}$	667	$\{(0,0,\gamma),(0,0,1)\}$
ω_{o2}	0	$\{(0,0,1),(0,0,1)\}$	568	$\{(0,0,0),(0,0,1)\}$	461	$\{(0,0,\gamma),(0,0,-1)\}$

tions of a C-C bond in which the fourth nearest neighbor C1 and C2 atoms in C1-C-C-C2 are vibrating. When we compare Table I with the previous force constants in parentheses,[5] the radial force constants for the second and third-nearest neighbors of Table I become relatively weak, and the tangential force constants become relatively hard, reflecting some modification to the values of the optical phonon modes.

B. Analytic expressions for the phonon modes

With the 12 force-constant parameters, we can solve the phonon frequencies at a **k** point by solving the 6×6 dynamical matrix.[5] If we can get some relationship between the force constants and phonon frequencies at some high symmetry points, the fitting procedures will be simplified. Force-constant sum rules are conditions that give a zero phonon frequency for the translational and rotational motion at $q=0$.[5,23] This condition is included by generating the force-constant tensors through rotation of one initial force-constant tensor. Another relationship is related to the eigenstates at high symmetry points where the phonon frequencies are given by a simple formula for the force constants, which decouples the problem into a smaller number of fitting parameters. Although we do not directly use these equations, they will be useful for understanding the various phonon dispersion relations of sp^2 carbons.

Here we show some analytical results of the phonon eigenmodes that are analytically determined as functions of the 12 force constants. An analytical calculation of the diagonalization of the 6×6 dynamical matrix is solved by MATHEMATICA at the three high symmetry points of 2D graphite BZ (Γ, K, and M).[5] For the 18 eigenvalues, three are acoustic phonon modes with zero frequency, which are independent of the force constants and the other three are doubly degenerate phonon modes, which is consistent with group theoretical arguments,[7] and are independent of the set of force constants that are used. Thus we get 12 formulas, which consist of eight in-plane and four out-of-plane modes, as shown in the Appendix. Since the in-plane and out-of-plane phonon modes are orthogonal in the graphene plane, the corresponding eigenvalues are given, respectively, in terms of in-plane and out-of-plane force constants. The conversion constant from a force constant in dyn/cm to a phonon

frequency in cm^{-1} is given by $\mathcal{C}=1.189\,28$ (cm^{-1}/dyn)$^{1/2}$. In Table II, we list the corresponding phonon frequencies and normal modes, which are obtained by the set of fitted force constants.

For the Γ point, the in-plane tangential phonon frequencies ω_{i1} and ω_{i2} are degenerate at 1589 cm^{-1}. This degeneracy comes from the facts that graphite is not an ionic crystal and that there is a threefold symmetry around each carbon atom.[5] For all phonon modes at the Γ point, all A (or B) atoms in the unit cells of 2D graphite move in the same phase, and, therefore, no second-nearest neighbor force constants $\Phi^{(2)}$ appear in the expressions (see the Appendix). Here, when we consider an $A(B)$ atom for the central atom, the first, the third, and the fourth-nearest neighbors are $B(A)$ atoms, while the second-nearest neighbors are $A(B)$ atoms.

For the K point modes, the in-plane tangential optic phonon modes (ω_{i2}, ω_{i3}) and the tangential out-of-plane modes (ω_{o1}, ω_{o2}) are degenerate. At the K point, either the A, or B atoms move in the normal mode eigenfunction, while the other atoms do not move. A similar situation appears, also, in the case of the electronic wave functions, where either the A, or B, components of the Bloch functions in the eigenfunctions have the proper value at the K points. It is interesting to see the result in the Appendix, that the degenerate eigenvalues are expressed by eigenvalues at the Γ points and the second-nearest neighbor force constant. The reason why a second-nearest neighbor force constant appears here is that the direction of the movement of the two second-nearest neighbors is not parallel. At the M point, both the A and B atoms move in the eigenfunctions differently, and thus all force constants appear mixed and no eigenstates are degenerate.

Although we have 12 relations between nonzero phonon frequencies at the high symmetry points and 12 unknown force constants, we cannot solve directly for all of the 12 force constants. The number of independent equations of the 12 equations in the Appendix is nine, which is understood in terms of the rank of the matrix for the 12 simultaneous equations. This means that three dependent equations between phonon frequencies at the different symmetry points exist. After some analytic calculation, we get the following three relations:

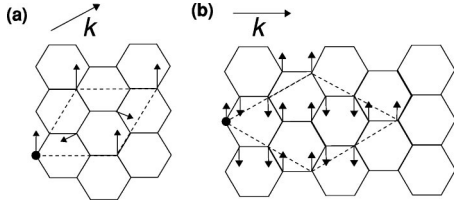$$\omega_{i1}(K)^2 + \omega_{i4}(K)^2 - 2\omega_{i2}(K)^2 = 0, \qquad (3)$$

FIG. 4. (a) Eigenvectors $\{(0,0,0),(-i,1,0)\}$ of $\omega_{i2}(K)$ $=1272$ cm^{-1}, which is the phonon branch corresponding to the D band, and (b) eigenvectors $\{(0,\gamma,0),(0,1,0)\}$ of $\omega_{i2}(M)$ $=1369$ cm^{-1}. The dashed diamond of each figure is the supercell for the K and M points. The arrows outside of the hexagonal lattice show the directions of the **k** vectors.

$$2\omega_{i1}(\Gamma)^2 - 9\sum_{j=1}^{4} \omega_{ij}(M)^2 + 32\omega_{i2}(K)^2 = 0 \tag{4}$$

and

$$\omega_{o1}(\Gamma)^2 - 9\sum_{j=1}^{2} \omega_{oj}(M)^2 + 16\omega_{o1}(K)^2 = 0. \tag{5}$$

These equations are independent of the set of force constants and thus they are useful for estimating the data that yield the phonon dispersion relations over the whole BZ of 2D graphite. Hopefully these results can also be applied to improve the present status of understanding of the phonon-related properties of carbon nanotubes.

In Fig. 4, we show examples of the eigenstates for the in-plane optic phonon modes for (a) $\omega_{i2}(K)$ and (b) $\omega_{i2}(M)$ whose phonon frequencies are 1272 and 1369 cm^{-1}, respectively. Starting from a lattice point of the B atom denoted by solid circles in Fig. 4, the vibrations of other atoms are given by multiplying the factor $\exp(i\mathbf{q}\cdot\mathbf{R})$ by the complex eigenfunctions of the unit cell of 2D graphite as shown in Table II when we shift the vibration by a lattice vector **R**. For the **q** vectors at the K and M points, the vibration has a periodicity, respectively, of the $\sqrt{3}\times\sqrt{3}$ and 2×2 supercells of 2D graphite, which are shown by dotted lines in Fig. 4. In Table II we show the eigenfunctions of four in-plane modes and two out-of-plane modes with calculated eigenvalues at Γ $=(0,0)$, $K=(2\pi/\sqrt{3}a,2\pi/3)$, and $M=(2\pi/\sqrt{3}a,0)$. The eigenvectors have six components: x,y,z for the A and B atoms of 2D graphite: $\{(A_x,A_y,A_z),(B_x,B_y,B_z)\}$. All eigenvectors at the symmetry points show the required symmetry between the A and B atoms, in which the normal modes for each atom are normalized to unity. All vectors have a length of unity, and the real part of the eigenfunction corresponds to the vectors shown in Fig. 4. In the 2D BZ, we have two inequivalent K and K' points, and three inequivalent M, M', and M'' points. The corresponding eigenfunctions are given by the rotational operations of 2D graphite in **k** space.

Since the eigenfunctions near the K and K' points show a large amplitude for either the A or B atoms, the localized phonon modes with a single missing atom have a frequency similar to that of the K point phonon modes. We see a localized phonon around a point defect, and the vibrational amplitude around the defect becomes large when its phonon-mode frequency is close to that of a D-band phonon

frequency mode. The same situation appears at the edge of a nanographite cluster where only A (or B) atoms are present at the so-called zigzag edge.[24] On the other hand, at the armchair edge, an even number of A and B atoms exists, which favors Γ point phonon eigenfunctions for constructing localized phonon modes. It would be interesting to compare the Raman intensity for the dispersive phonon modes from different types of defects, and this will be addressed in future work.

V. SUMMARY

In summary, we fit the dispersive phonon modes around the K and Γ points to the phonon dispersion relations in a self-consistent way. The optical phonon modes of the phonon dispersion relations near the K point are modified by the fitting to new experimental data, and the results can be checked by further experimental observations. We also give analytic expressions for the eigenvalues and eigenfunctions of the 2D graphite phonon modes at the high symmetry points. The analytic expressions for the phonon eigenvalues are useful for decoupling the fitting procedure for different force constants, while the direction of the eigenfunctions is determined only by symmetry at the high symmetry points. We found some dependent equations between phonon frequencies at high symmetry points, which will be useful for checking the calculation and for estimating phonon frequencies from known values. Second-order Raman spectra thus have provided new force-constant sets that will cover the phonon dispersion relations over the whole BZ of 2D graphite and will also apply to the phonon properties of carbon nanotube.

APPENDIX: ANALYTIC EXPRESSIONS OF EIGENVALUES OF 2D GRAPHITE

Analytic expressions for the phonon frequencies for the 2D graphite phonon modes are given here for the three high symmetry points in graphite. $\mathcal{C}=1.18928$(cm^{-1}/dyn)$^{1/2}$ is the conversion constant from a force constant in dyn/cm to a phonon frequency in cm^{-1}. The phonon frequencies at the Γ point are as follows

$$\omega_{i1}(\Gamma) = \mathcal{C}\sqrt{3\Phi_r^{(1)} + 3\Phi_{ti}^{(1)} + 3\Phi_r^{(3)} + 3\Phi_{ti}^{(3)} + 6\Phi_r^{(4)} + 6\Phi_{ti}^{(4)}},$$

$$\omega_{o1}(\Gamma) = \mathcal{C}\sqrt{6\Phi_{to}^{(1)} + 6\Phi_{to}^{(3)} + 12\Phi_{to}^{(4)}}.$$

The phonon frequencies at the K point are given as

$$\omega_{i2}(K) = \sqrt{0.5[\omega_i(\Gamma)^2 + 9\mathcal{C}^2(\Phi_r^{(2)} + \Phi_{ti}^{(2)})]}$$

$$\omega_{i1}(K) = \sqrt{\omega_{i1}(K)^2 - \Delta},$$

$$\omega_{i4}(K) = \sqrt{\omega_{i1}(K)^2 + \Delta},$$

with

$$\Delta = \mathcal{C}^2\{1.5(\Phi_r^{(1)} - \Phi_{ti}^{(1)} + \Phi_r^{(3)} - \Phi_{ti}^{(3)}) - 2.79(\Phi_r^{(4)} - \Phi_{ti}^{(4)})\}$$

$$\omega_{o1}(K) = \sqrt{9\mathcal{C}^2\Phi_{to}^{(2)} + 0.5\omega_{o1}^2(\Gamma)}.$$

The phonon frequencies at the M point are given by

$$\omega_{i1}(M) = \mathcal{C}(2\Phi_r^{(1)} + 6\Phi_r^{(2)} + 2\Phi_{ti}^{(2)} + 3\Phi_r^{(3)} + 3\Phi_{ti}^{(3)}$$
$$+ 2.29\Phi_r^{(4)} + 1.71\Phi_{ti}^{(4)})^{(1/2)},$$

$$\omega_{i2}(M) = \mathcal{C}(\Phi_r^{(1)} + 3\Phi_{ti}^{(1)} + 6\Phi_r^{(2)} + 2\Phi_{ti}^{(2)} + 3.71\Phi_r^{(4)}$$
$$+ 4.29\Phi_{ti}^{(4)})^{1/2},$$

$$\omega_{i3}(M) = \mathcal{C}(3\Phi_r^{(1)} + \Phi_{ti}^{(1)} + 2\Phi_r^{(2)} + 6\Phi_{ti}^{(2)} + 4.29\Phi_r^{(4)}$$
$$+ 3.71\Phi_{ti}^{(4)})^{(1/2)},$$

$$\omega_{i4}(M) = \mathcal{C}(2\Phi_{ti}^{(1)} + 2\Phi_r^{(2)} + 6\Phi_{ti}^{(2)} + 3\Phi_r^{(3)} + 3\Phi_{ti}^{(3)}$$
$$+ 1.71\Phi_r^{(4)} + 2.29\Phi_{ti}^{(4)})^{(1/2)},$$

$$\omega_{o1}(M) = \mathcal{C}\sqrt{4\Phi_{to}^{(1)} + 8\Phi_{to}^{(2)} + 8\Phi_{to}^{(4)}},$$

$$\omega_{o2}(M) = \mathcal{C}\sqrt{2\Phi_{to}^{(1)} + 8\Phi_{to}^{(2)} + 6\Phi_{to}^{(3)} + 4\Phi_{to}^{(4)}}.$$

[1] R.A. Jishi, L. Venkataraman, M.S. Dresselhaus, and G. Dresselhaus, Chem. Phys. Lett. **209**, 77 (1993).

[2] N. Wakabayashi, R.M. Nicklow, and H.G. Smith, Phys. Rev. B **5**, 4951 (1972).

[3] T. Aizawa, R. Souda, S. Otani, Y. Ishizawa, and C. Oshima, Phys. Rev. B **42**, 11 469 (1990).

[4] R.E. Palmer, J.L. Wilkes and R.F. Willis, J. Electron Spectrosc. Relat. Phenom. **44**, 355 (1987).

[5] R. Saito, G. Dresselhaus, and M. S. Dresselhaus, *Physical Properties of Carbon Nanotubes* (Imperial College Press, London, 1998).

[6] S. Siebentritt, R. Pues, K.-H. Rieder, and A.M. Shikin, Phys. Rev. B **55**, 7927 (1997).

[7] C. Mapelli, C. Castiglioni, G. Zerbi, and K. Müllen, Phys. Rev. B **60**, 12 710 (1999).

[8] R. Saito, T. Takeya, T. Kimura, G. Dresselhaus, and M.S. Dresselhaus, Phys. Rev. B **57**, 4145 (1998).

[9] M.S. Dresselhaus and P.C. Eklund, Adv. Phys. **49**, 705 (2000).

[10] R. Saito, A. Jorio, A.G. Souza Filho, G. Dresselhaus, M.S. Dresselhaus, and M.A. Pimenta, Phys. Rev. Lett. **88**, 027401 (2002).

[11] F. Tuinstra and J.L. Koenig, J. Chem. Phys. **53**, 1126 (1970).

[12] M. S. Dresselhaus, G. Dresselhaus, A. Jorio, A. G. Souza Filho, and R. Saito, Carbon (to be published 2002).

[13] M.A. Pimenta, E.B. Hanlon, A. Marucci, P. Corio, S.D.M. Brown, S.A. Empedocles, M.G. Bawendi, G. Dresselhaus, and M.S. Dresselhaus, Braz. J. Phys. **30**, 423 (2000).

[14] M.J. Matthews, M.A. Pimenta, G. Dresselhaus, M.S. Dresselhaus, and M. Endo, Phys. Rev. B **59**, R6585 (1999).

[15] C. Thomsen and S. Reich, Phys. Rev. Lett. **85**, 5214 (2000).

[16] J. Kürti, V. Zólyomi, A. Grüneis, and H. Kuzmany (unpublished).

[17] R. M. Martin and L. M. Falicov, in *Light-Scattering in Solids*, edited by M. Cardona (Springer-Verlag, Berlin, 1975), p. 80.

[18] L. G. Cançado, M. A. Pimenta, R. Saito, A. Jorio, L. O. Ladeira, A. Grüneis, A. G. Souza Filho, G. Dresselhaus, and M. S. Dresselhaus (unpublished).

[19] Y. Kawashima and G. Katagiri, Phys. Rev. B **52**, 10 053 (1995).

[20] Y. Kawashima and G. Katagiri, Phys. Rev. B **59**, 62 (1999).

[21] P.H. Tan, C.Y. Hu, J. Dong, W. Shen, and B. Zhang, Phys. Rev. B **64**, 214301 (2001).

[22] P.-H. Tan, Y. Tang, Y.-M. Deng, F. Li, Y.L. Wei, and H.M. Cheng, Appl. Phys. Lett. **75**, 1524 (1999).

[23] O. Madelung, *Solid State Theory* (Springer-Verlag, Berlin, 1978).

[24] K. Nakada, M. Fujita, G. Dresselhaus, and M.S. Dresselhaus, Phys. Rev. B **54**, 17 954 (1996).

[25] R. Al-Jishi and G. Dresselhaus, Phys. Rev. B **26**, 4514 (1982).